Construction, characterization, and immunization of nanoparticles that display a diverse array of influenza HA trimers

Alexander A. Cohen[1], Zhi Yang[1], Priyanthi Gnanapragasam[1], Susan Ou[1], Kim-Marie Dam[1], Haoqing Wang[1,2], Pamela J. Bjorkman[1*]

[1]Division of Biology and Biological Engineering, California Institute of Technology, Pasadena, CA 91125, USA

[2]Present address: Department of Cellular Physiology and Medicine, Stanford University School of Medicine, Palo Alto, CA 94305, USA

*Corresponding author: Email: bjorkman@caltech.edu

Abstract

Current influenza vaccines do not elicit broadly protective immune responses against multiple strains. New strategies to focus the humoral immune response to conserved regions on influenza antigens are therefore required for recognition by broadly neutralizing antibodies. It has been suggested that B cells with receptors that recognize conserved epitopes would be preferentially stimulated through avidity effects by mosaic particles presenting multiple forms of a variable antigen. We adapted SpyCatcher-based platforms, AP205 virus-like particles (VLPs) and mi3 nanoparticles (NPs), to covalently co-display SpyTagged hemagglutinin (HA) trimers from different influenza strains. Here we show successful homotypic and heterotypic conjugation of up to 8 different HA trimers to both VLPs and NPs, and demonstrate that conjugated particles were stable for several weeks of storage. We characterized the HA-VLPs and HA-NPs by cryo-electron tomography to derive the average number of conjugated HAs and their separation distances, and compared immunizations of mosaic and homotypic particles in wild-type mice. Both types of HA particles elicited strong antibody responses, but the mosaic particles did not consistently elicit broader immune responses. We conclude that covalent attachment of HAs from currently-circulating influenza strains represents a viable alternative to current annual influenza vaccine strategies, but in the absence of further modifications, is unlikely to represent a method for making a universal influenza vaccine.

Key words: Influenza virus, Hemagglutinin nanoparticles, Hemagglutinin VLPs, SpyCatcher, Nanoparticle vaccine, Immunizations, Cryo-electron tomography

Introduction

Each year, influenza virus infections affect 5-30% of the global population, resulting in millions of severe infections and hundreds of thousands of deaths [1]. Yearly epidemics are typically caused by the influenza type A, with a smaller number of infections resulting from type B. Vaccines can minimize the incidence of severe infections; however, they do not offer complete protection and have to be re-administered annually [1, 2]. The lack of complete efficacy of current vaccines can be attributed to several reasons. Mainly, the virus undergoes antigenic drift in which mutations accumulate over time that can allow the virus to evade the humoral immune response [1]. This requires that the vaccine formulation be renewed yearly so that the vaccine strains match the circulating strains as closely as possible. Influenza virus also features high antigenic diversity resulting in predominantly strain-specific antibody responses and making it difficult to recognize conserved regions on the viral antigens [2, 3]. Furthermore, through the mechanism of antigenic shift, the RNA segments from strains of different origins can reassort, resulting in new strains that are typically the cause of global pandemics that can rapidly circulate within an antigenically-naïve population [1]. Altogether, these necessitate the need for a universal flu vaccine that could confer protection against a broad swath of antigenically-distinct strains, thereby eliminating the need for yearly vaccines and offering protection against emergent pandemics.

The antibody response to influenza is primarily directed against the hemagglutinin (HA) and neuraminidase (NA) glycoproteins, which appear as a dense array of spikes on the surface of the viral particles [3, 4]. The majority of the neutralizing antibody response is against HA, the most abundant viral surface glycoprotein and the sialic acid-binding receptor that mediates fusion between the viral and host membranes. Influenza HA is a trimer of HA1 and HA2 heterodimers, which can be subdivided into head and stalk domains [3, 4]. The HA head is composed of the middle portion of the HA1 sequence, contains the sialic acid binding site responsible for host cell recognition, and features high variability between different strains/subtypes. The HA2 subunit along with N- and C-terminal regions of HA1 encodes for the more conserved stalk domain, which contains the fusion peptide involved in viral/host cell membrane fusion [3, 4]. Antibodies against the immunodominant HA head can be strongly neutralizing, but are also strain specific, with the exception of antibodies that recognize the receptor binding site [3, 5, 6]. In contrast, the HA stem is immunosubdominant; however, stem antibodies are often broader, although generally less potent than anti-head antibodies, and can induce antibody-dependent cellular cytotoxicity (ADCC) responses [3, 7-9]. Within the past 10 years, broadly neutralizing antibodies (bNAbs) against influenza that target conserved HA stem epitopes have been discovered, but these antibodies have thus far been difficult to elicit [10]. It is generally believed that a broadly protective or “universal” vaccine would require the induction of anti-HA stem antibodies. As a result, there have been numerous attempts to refocus the immune response to these conserved epitopes [11-16].

One strategy to redirect the antibody response towards invariant epitopes was co-displaying influenza HAs from different strains on nanoparticles [16]. The rationale was to display HAs from several strains on a multimerized platform, such that any two adjacent HAs have a low probability of being identical, thereby giving a competitive advantage to B cells with B cell receptors (BCRs) that use avidity effects to recognize conserved epitopes shared between different strains. By contrast, BCRs that recognize strain-specific epitopes could not use avidity effects to bind adjacent HAs, thus would be less likely to be activated [16]. In this study, monomeric HA receptor binding domain (RBD) sequences were fused to an engineered ferritin subunit to create self-assembling particles displaying up to eight different RBD sequences derived from H1N1 strains at 24 total positions. The elicited humoral immune response in injected mice featured high breadth and potency against a panel of diverse H1N1 strains, which

was most apparent the larger the number of HAs that were co-displayed, such that the simultaneous display of 8 different HAs elicited the greatest breadth in comparison with immunization of a cocktail of 8 different homotypic HA nanoparticles. Sorting and isolation of memory B cells that were positive for HAs from two different strains further supported the use of this strategy for inducing cross-reactive B cells. A logical follow up to this study would be to co-display HA ectodomain trimers including the stalk and head regions instead of RBD head domain monomers, with the hope of eliciting antibody lineages with increased breadth.

We reasoned that co-display of multiple HA trimers on a nanoparticle would be facilitated by a system in which soluble HA trimers could be covalently attached to a protein nanoparticle, thereby avoiding potential folding problems created by genetically fusing protomers from a trimer to a nanoparticle subunit. Numerous NP platforms and coupling strategies have been explored for vaccine design [17]. The “plug and display” strategy involves the use of virus-like particles (VLPs) or nanoparticles (NPs) fused to a SpyCatcher protein that is covalently conjugated to a purified antigen tagged with a short (13-residue) SpyTag [18, 19]. The conjugation involves the formation of an isopeptide bond between a lysine from the SpyCatcher protein and an aspartate from the Spytag [20]. An advantage of the SpyCatcher-SpyTag system is that it allows for the spontaneous irreversible conjugation of a purified antigen with native-like post-translational modifications to a scaffold via an incubation of the antigen and scaffold proteins under physiological conditions. Available SpyCatcher protein scaffolds are highly versatile, coming in different forms that range from a bacteriophage AP205 T=3 icosahedral particle (180 SpyCatchers) to a designed dodecahedral NP called mi3 (60 SpyCatchers) [18, 19]. We recently used AP205 SpyCatcher-VLPs to display SpyTagged trimeric HIV-1 Env immunogens and demonstrated priming in immunized mice and non-human primates of B cells carrying receptors displaying characteristics of V3-glycan patch-targeting HIV-1 bNAbs [21].

Here we describe the use of bacteriophage AP205-based SpyCatcher VLPs and engineered particle mi3-based SpyCatcher NPs [18, 19] to display a diverse array of HA ectodomain trimers from Group 1 and Group 2 influenza A strains. Successful conjugation was demonstrated by size-exclusion chromatography, SDS-PAGE, and electron microscopy (EM), with up to eight different HA trimers successfully conjugated to make mosaic mi3 particles. The coupled particles are stable upon storage for at least one month at 4˚C. Cryo-electron tomography (cryo-ET) revealed 81-144 conjugated HA trimers per AP205 VLP and 18-24 trimers per mi3 NP, with average separation distances between HA trimers ranging from 7-10 nm for the AP205 VLPs to 12-15 nm for the mi3 NPs. Immunization studies using a mosaic HA-VLP with a valency of two (mosaic-2 VLP) were performed in wild-type (wt) mice and compared to mice immunized with a mixture of two homotypic VLPs (admix-2 VLPs). Serum ELISAs and neutralization assays from immunized mice revealed roughly equivalent breadth and potency for responses to the mosaic-2 and admix-2 VLPs against a panel of influenza A strains. HA-mi3 NPs were used in a second immunization experiment (mosaic-2, -4, or -8 versus admix-2, -4, or -8), which exhibited roughly equivalent breadth with an exception in one mouse, suggesting the possibility of greater breadth achieved by injection of mosaic particles.

These results demonstrate that SpyCatcher-VLPs and SpyCatcher NPs can be easily used to stably display at least 8 different trimeric antigens. Both AP205-HA and mi3-HA particles produced strong immune responses in mice. Our biochemical and EM imaging analyses of HA-VLP and HA-NP particles provide useful characterizations for future efforts to utilize the SpyCatcher-SpyTag system for homotypic and heterotypic display of oligomeric antigens.

Results and Discussion

Construction of HA-VLPs and HA-NPs. We adapted the AP205 SpyCatcher-VLP platform that we had previously used to conjugate a trimeric HIV-1 immunogen [21] as a way to increase the intrinsic immunogenicity of HA, mask undesired epitopes located at the bottom of the HA trimer, and potentially attach different HA trimers to the same particle. We reasoned that the SpyCatcher-VLP platform could be used to display more than one HA by incubating with equimolar amounts of different SpyTagged HAs. Although the SpyTagged HAs would be conjugated at random to available SpyCatcher proteins, there should be no advantage for the conjugation of one HA over another since they all contained the same SpyTag.

We first expressed and purified SpyTagged soluble HA trimers derived from 8 different influenza strains (Figure 1A). The constructs for each HA protomer contained HA1 and the HA2 ectodomain (residue 1-503 H3 numbering) linked to a C-terminal foldon trimerization domain, a SpyTag and a 6x-His tag (Figure 1A). The HAs for the SpyCatcher-mi3 conjugations included the sialic acid binding knockout mutation Y98F (except for the SpyTagged HAs used to conjugate the SpyCatcher-VLPs). SpyTagged HAs including the Y98F substitution purified from the supernatants of transiently-transfected mammalian cells were verified to form monodisperse and well-behaved trimers by SEC and SDS-PAGE (Figure 1B). We used SpyCatcher-AP205 VLPs and SpyCatcher-mi3 NPs as conjugation platforms for multivalent display of HA trimers. AP205-SpyCatcher VLPs are icosahedral capsids (T=3 symmetry) with 180 copies total, therefore 180 Spycatchers for conjugation (Figure 1C). AP205-SpyCatcher VLPs were expressed in *E. coli* and purified via Ni-NTA affinity chromatography followed by SEC (Figure 1D) [18]. The Spycatcher-AP205-VLPs eluted near the void volume as a single monodisperse peak. SpyCatcher-mi3 NPs are a dodecameric engineered scaffold with 60 total subunits, therefore 60 conjugation sites (Figure 1E). The SpyCatcher-mi3s were also expressed in *E. coli*, purified by Ni-NTA affinity chromatography followed by SEC, and analyzed with reducing SDS-PAGE (Figure 1F).

Using the SpyCatcher-AP205 VLPs, we first evaluated coupling of two recombinant HAs, A/California/04/09 H1 (CA09-HA) and A/Aichi/02/1968 H3 (Aichi-HA) (chosen to represent two strains that would normally be present in an annual influenza vaccine). Conjugations of the AP205-Spycatcher VLPs were carried out by room temperature incubation with CA09-HA, Aichi-HA, or an equimolar mixture of both HAs in a 1.2 molar excess to the VLPs (HA protomer to VLP subunit) to prepare CA09-, Aichi-, and mosaic-2 VLPs, respectively (Figure 2A). VLP-conjugated HA trimers were separated from free trimers by SEC (Figure 2B), and successful conjugation of the SpyCatcher VLPs to Aichi-HA, CA09-HA, and both HAs was verified by a shift in apparent molecular weight (from 75 kDa to 100 kDa) detected by SDS-PAGE for HAs conjugated to the VLP subunits (Figure 2B).

Because VLPs conjugated with more than two different HAs tended to precipitate out of solution (data not shown), we switched to the SpyCatcher mi3 platform, which is similarly immunogenic as the AP205 platform, but has been shown to exhibit improved yields, stability, and uniformity [19]. In addition, we modified the SpyTagged HAs to include a receptor binding site mutation, Y98F (H3 numbering), to abolish sialic acid binding [22] that could result in interactions of aggregation of HAs on neighboring particles. Starting with 8 HAs from influenza group 1 and group 2 strains (Figure 1A) with pandemic potential [23], we made mosaic-2, mosaic-4 and mosaic-8 mi3 NPs (each with an equal representation of group 1 and group 2 strains) and the 8 corresponding homotypic HA-conjugated NPs (Figure 2C). Homotypic HA-mi3s were purified via SEC, and conjugation was verified by a shift in apparent molecular weight (from 75 kDa to >100 kDa) detected by SDS-PAGE for HAs conjugated to the mi3 subunits (Figure 2D). Mosaic-mi3 NPs were purified and analyzed the same way (Figure 2E). Finally, to assess stability of the

conjugated NPs, mosaic-NP preps stored for 1 month at 4˚C were analyzed for degradation by SEC, revealing little to no free HA trimer for both the mosaic-4 and mosaic-8 NPs.

EM characterization of HA-VLPs and HA-NPs

Negative-stain EM revealed increased diameters for conjugated VLPs and NPs compared with their unconjugated counterparts (Figure 3A). HA-conjugated VLPs were also examined by single-particle cryo-EM. 2D class averages of mosaic-2 VLPs showed ordered density for the AP205 VLP, but blurred densities for attached HAs (Figure 3B), suggesting variability in trimer orientations with respect to the VLP surface.

Since the HA trimer densities could not be reliably interpreted by single-particle cryo-EM, we used cryo-ET to derive 3D reconstructions of individual HA-conjugated VLPs and NPs. Tomograms (Supplemental Movies 1 and 2) showed particles with average diameters of 60 nm (HA-VLPs) and 50 nm (HA-NPs) and revealed densities for individual HA trimers on VLPs and NPs. The trimers were separated by distances of ~7-10 nm and ~12-15 nm for VLPs and NPs, respectively (measured between the head regions of trimer axes on adjacent HAs). To estimate the number of conjugated HA trimers, we counted HA densities in ~3 nm tomographic slices of individual HA-VLPs and HA-NPs at their widest diameters, where the symmetries of each type of particle predicted a maximum of 20 potential attachment sites. We found 9-16 HA densities for conjugated VLPs and 6-8 densities for conjugated NPs, corresponding to occupancies of 45-80% (VLPs) and 30-40% (NPs). Since AP205 VLPs and mi3 NPs contain 180 or 60 SpyCatchers, respectively, this translates to ~81-144 conjugated HA trimers per AP205 VLP and ~18-24 trimers per mi3 NP.

Immunizations with homotypic- and mosaic-HA-VLPs. Our next goal was to determine whether mosaic HA-VLPs induced a more cross-reactive humoral immune response compared with a mixture of the corresponding homotypic HA-VLPs. We first immunized one group of four mice with mosaic-2 VLPs (presenting CA09 plus Aichi HAs) and a second group of four mice with an equal mixture of CA09-VLPs and Aichi-VLPS (admix-2) (Figure 4A). In addition, we immunized groups of mice with only Aichi-VLPs or only CA09-VLPs. In all cases, mice were primed with equal doses of VLPs plus adjuvant, boosted 2 weeks later without adjuvant, and bled weekly for serum analyses.

Serum ELISAs were performed to measure IgG binding to purified HAs from a panel of Group 1 and Group 2 influenza A strains (Figure 4B). For the Aichi and CA09 HAs presented on the VLPs, IgG titers from mosaic-2- and from admix-2-immunized mice were equivalent and similar to titers against CA09 HA for CA09-VLP-injected mice and against Aichi HA for Aichi-VLP-injected mice. Against heterotypic HAs not presented on the VLPs (Viet04, Jp57, WF10, Sh13 and JX346 HAs), IgG titers were equivalent for both mosaic-2- and admix-2-immunized mice, although titers were increased compared with both CA09-VLP- and Aichi-VLP-immunized mice. Thus in terms of elicited IgG binding of HAs, it appeared that immunizing with the mosaic-2 VLPS was no better at inducing cross-reactive binding of HAs from divergent strains than the corresponding admixture. However, the mosaic-2 and admix-2 injections seemed to induce heterologous breadth that could not be explained by the overlapping immunogenicities of the homotypic VLPs.

Neutralizing activity of the serum was determined using in vitro neutralization assays (using live viruses for BSL 2 strains and pseudoviruses for BSL 3 strains) against a panel of Group 1 and Group 2 influenza A strains (Figure 4C). For the mosaic-2- and admix-2-immunized mice, neutralizing titers against homotypic live virus strains (CA09 and Aichi) were consistent with the ELISA titers against these strains. Against the Viet04 and JX346 pseudoviruses, neutralization

titers are not detectable except from one animal in the admix-2 group. Against the Sh13 pseudovirus, neutralizing titers for the mosaic-2-immunized mice were higher than for the other groups, although the spread in potency was broad and overlapped with the other groups. Altogether in terms of neutralization, it appeared that immunizing with the mosaic-2 VLPs may have induced antibodies with slightly higher breadth than for the admixture of homotypic VLPs, when considered together with the ELISA results, the mosaic-2 VLPs were not better than the homotypic VLPs in eliciting breadth.

In order to determine whether mosaic-HA NPs with higher valencies could elicit antibody responses with higher breadth, we conducted experiments similar to those described for VLPs to compare injections of mosaic-2, -4 and -8 NPs with the corresponding admixtures of homotypic NPs (Figure 5A), with a CA09-NP homotypic control, and with unconjugated SpyCatcher-NPs. A final boost was performed 5 weeks after the first prime and animals were sacrificed 2 weeks later to harvest spleens for B cell analysis. Serum IgG titers from Day 21 and Day 49 were measured using ELISAs against a panel of purified HAs from homotypic and heterotypic Group 1 and Group 2 strains (Figure 5B) and against unconjugated SpyCatcher-mi3 NPs. All groups of mice exhibited antibody responses to unconjugated SpyCatcher-mi3, suggesting that SpyCatcher and/or NP epitopes are accessible on HA-conjugated particles.

Against HAs from homotypic strains (CA09 and Aichi), the serum from mice immunized with both the admix and mosaic NPs featured equivalent titers, with the exception of the admix-4 mouse group, which responded with overall lower titers and included 2 mice with no responses. Against the Viet04 and JX346 HAs (presented on particles with valencies of 4 and 8), the response was slightly higher for the mosaic-2 NPs than for the Ca09-mi3 and admix-2 groups, whereas the mosaic-4, mosaic-8 and admix-8 groups showed higher titers, although over a broad range that included mice with poor responses even against strains of HA that were presented on admix-4 NPs. Against the Jp57, JX346, WF10, and HB09 HAs (only present on the valency-8 NPs), the admix-8 and mosaic-8 titers were equivalent to each other and the highest on average. The titers against heterologous HAs from the CA09-mi3-injected mice were similar to titers from mice injected with SpyCatcher-mi3 NPs, with the exception of responses against Jp57 HA. Responses to the mosaic-2 NPs were slightly higher than responses against admix-2 and CA09-mi3, again except for the recognition of Jp57 HA. One animal in the mosaic-4 group exhibited high titers against HAs from all strains in comparison to the admix-4 mice, with the mosaic-4 responses being on par with responses from the animals immunized with the valency-8 NPs. Finally, against HAs from Pe10 and WA79 (not presented on the any of the NPs), serum titers were low for most of the injected animals except for some animals from the mosaic-4 group (e.g., the animal that exhibited high titers against strains not represented on the mosaic-4 NPs), and admix-8- and mosaic-8-immunized mice.

ELISAs were also used to evaluate recognition of CA09-miniHA, a stabilized stem-only construct derived from CA09 HA [11] to ask whether there was preferred recognition of stem epitopes by the animals immunized with mosaic-NPs. We found that the serum response against the CA09 stem was equivalent to responses against the head-containing CA09 HA trimer, with the CA09-mi3-immunized mice exhibiting the highest titers (Figure 5B), suggesting that the mosaic-NPs did not preferentially elicit anti-stem responses.

ELISA titers determined for serum samples obtained on Day 51 showed similar responses as Day 21 titers with a few exceptions. For example, the mosaic-8 NP-immunized mice had lower titers with respect to the admix-8 mice against some of the HAs, suggesting that the boosts were not consistently resulting in strong immune responses. The mice immunized with the mosaic-4 NPs mounted more robust responses, although two of the animals exhibited low titers

against all of the strains (as compared with three animals from Day 21). Based on ELISA binding results, we did not find strong evidence of increased cross-reactivity induced in animals immunized with the mosaic NPs compared with animals injected with the corresponding admix-NPs of the same valency. However, for the mosaic-4 NP group, one animal repeatedly showed high titers of IgG binding to HAs from all strains tested, suggesting that this animal may have induced cross-reactive antibodies. The caveat is that the number of animals in this experiment was low, so that results from animals that responded poorly to immunogenic challenge lowered the average titers, even though cross-reactive antibodies may have been elicited in at least one animal in this group.

In vitro neutralization assays were also conducted using Day 51 serum against a panel Group 1 and Group 2 influenza strains (Figure 5C). For CA09, neutralization titers were consistent with the ELISA titers, with Ca09-mi3-immunized mice showing the highest responses. The neutralizing response to Aichi also corresponded to the ELISA results. For the two heterotypic H1 and H3 HAs (TX91 and WI05 strains), serum from all animals was non-neutralizing, suggesting that neutralizing antibodies that cross-react within the H1 and H3 subtypes were not induced. For Viet04, Sh13 and NL03, the neutralizing responses were inconclusive and hard to interpret due to high background neutralization from the unconjugated mi3 control serum. For JX346, titers for the mosiac-2-immunized mice were higher in comparison to the admix-2-immunized mice, which exhibited no detectable neutralization activity. For mosaic-4-injected mice, serum from the same animal shown to bind to most strains by ELISA also showed a high neutralizing titer against the JX346 strain that was comparable to titers from the mosaic-8-immunized mice, which were injected with particles that presented JX346 HA. Overall, it appeared that the mosaic-NPs did not offer an advantage compared to corresponding mixtures of homotypic particles in induction of neutralizing antibodies, although the mosaic-4 and mosaic-2 groups included some animals in which some breadth was induced.

B cell responses induced by mosaic- versus homotypic-NP immunizations. In order to determine whether cross-reactive B cells were elicited during the immune response to mice immunized with the mosaic-NPs, IgG+ B cells from immunized mouse spleens were probed for binding to soluble HAs from three different influenza strains using flow cytometry (Figure 6A). The percent binding was determined by gating antigen-specific populations to compare populations positive for CA09, Viet04, or Aichi HAs alone, and for double-positive populations representing B cells that exhibited cross-reactivity (Figure 6B; Supplementary Figure 3). As expected, the percent CA09+ population was the largest for the CA09-mi3-immunized mice, with the rest of the mosaic and admix groups eliciting a similar proportion of the CA09+ B cells. Admix and mosaic groups with valencies of 4 and 8 elicited a similar levels of Viet04+ IgG+ B cells, as expected since Viet04 HA was present on these NPs. Interestingly, the mosaic-2-immunized mice elicited a somewhat lower, but detectable, number of Viet04+ B cells, which are not present in the admix-2 and homotypic CA09-mi3 samples. Except for the CA09-mi3-immunized mice, all animals showed Aichi+ B cells; however, the mosaic-2-immunized mice elicited the largest number, consistent with the ELISA and neutralization results (Figure 6A,B). Interestingly, very few CA09+/Viet04+ B cells were induced in immunized animals, with the exception of one animal in the mosaic-4-immunized group, which also featured a high serum IgG and neutralizing response. The CA09-mi3 and admix-8 immunized mice seem to have also induced double-positive B cells, although to a smaller extent. CA09+/Aichi+ and Viet04+/Aichi+ double-positive B cells were not detected for any of the animals (data not shown).

Taken together, our results suggest that immunizations with mosaic-NPs conjugated with HA trimers did not offer a clear advantage in the induction of cross-reactive B cells compared with immunization of mixtures of homotypic NPs. However, one animal immunized with the mosaic-4

NPs may have induced bona fide cross-reactive B cells that were not only shown to bind to two different HAs, but also produced serum that was cross-reactive by ELISA and in vitro neutralization with multiple strains of influenza (Figure 5B,C; 6B). Further immunization experiments on a larger cohort of animals will be required to determine if this result is reproducible in other animals before concluding that mosaic-VLPs induce better recognition of conserved HA epitopes.

Acknowledgements
We thank Mark Howarth (Oxford) for providing plasmids and advice for VLP expression and purification, Jesse Bloom (Fred Hutchinson) for reagents for the live virus neutralization assays, Jost Vielmetter and Pauline Hoffmann at the Caltech Protein Expression Center for help with protein production, Andrey Malyutin and Songye Chen (Caltech) for help with cryo-EM data collection, Rochelle Diamond and Jamie Tijerina at the Caltech Flow Cytometry/Cell Sorting Facility for help in the flow cytometry experiments and analysis, Jennifer Keeffe for implementation of influenza neutralization assays, Claudia Jette for help with figure preparation, Harry Gristick for VLP and NP images for figures, and Jennifer Keeffe and Claudia Jette for critical reading of the manuscript. EM was done in the Beckman Institute Resource Center for Transmission Electron Microscopy at Caltech. This work was supported by the National Institute of Allergy and Infectious Diseases of the National Institutes of Health Grant HIVRAD P50 AI150464 (PJB) and the National Institutes of Health Grant P50 GM082545-06 (PJB).

METHODS

Expression and purification of soluble HA trimers. HA ectodomain trimers were expressed as shown schematically in Figure 1A with a C-terminal foldon trimerization domain, 13-residue SpyTag [20], and a 6x-His (modified from HA constructs in [26] to include a SpyTag). Genes corresponding to the modified HA1-HA2 sequences (residues 1-504 H3 numbering) from A/Aichi/02/1968 (Aichi; H3), A/Shanghai/1/2013 (SH13; H7), A/Jiangxi-Donghu/346/2013 JX346; H10), A/swine/HuBei/06/2009 (HB09; H4), A/California/04/2009 (CA09; H1), A/Vietnam/1203/ 2004 (Viet04; H5), A/Japan/305/1957 (JP57; H2), and A/guinea fowl/Hong Kong/1999 (WF10; H9N2) were subcloned into a pTT5 vector expression vector. Genes encoding SpyTagged HAs with a Y98F mutation (H3 numbering) were constructed using site directed mutagenesis. HA ectodomain trimer constructs were expressed by transient transfection using the Expi293 Expression System (ThermoFisher), and soluble HA trimers were purified from transfected cell supernatants by standard Ni-NTA chromatography using a prepacked HisTrap™ HP column (GE Healthcare) and SEC using a HiLoad® 16/600 Superdex® 200 column (GE Healthcare). Proteins were concentrated using a Amicon Ultra 15 mL 30K concentrator (MilliporeSigma) and stored at 4 °C in 20 mM Tris pH 8.0, 150 mM NaCl, 0.02% NaN_3 (TBS buffer).

HA ectodomain trimers for ELISAs were expressed as above without the 13-residue SpyTag or the Y98F substitution. Additional strains only used for ELISA include: A/shearwater/West Australia/2576/79 (WA79; H15) and A/flat-faced bat/Peru/033/2010 (Pe10; H18). The CA09-miniHA construct [11] (construct #4900) was subcloned into a pTT5 vector with a 6x-His tag and expressed and purified as described for the HA ectodomain trimers. For flow cytometry experiments, an Avi-tag was inserted after the C-termini of the Aichi, Viet04, and CA09 HAs with the Y98F substitution. Avi-tagged HAs were expressed and purified as described above and biotinylated using the Biotin ligase kit (Avidity) according to the manufacturer's protocol. Biotinylated CA09-HA, Aichi-HA and Viet04-HA were incubated with eBioscience™ Streptavidin APC, Streptavidin PE-eFluor™ 610, or Streptavidin PE (ThermoFisher) overnight at 4°C at a 1:1 molar ratio of HA trimer to streptavidin subunit.

Expression of SpyCatcher-VLPs and SpyCatcher NPs. pGEN SpyCatcher AP205-CP3 for expression of SpyCatcher-VLPS was the kind gift of Dr. Mark Howarth (Oxford University). pGEN SpyCatcher AP205-CP3 was transformed into OverExpress™ C41(DE3) *E.coli* (Sigma). Single colonies were picked and inoculated into a 2xYT (Sigma) overnight starter culture and then grown in 1L 2xYT media with shaking at 220 rpm at 37˚C until OD 0.5 (A_{600}), after which they were induced with 0.42 mM IPTG and grown for 5 hours at 30˚C. Cultures were harvested and pellets were frozen in lysis buffer (20mM Tris-HCl pH 7.8, 150mM NaCl, 0.1% Tween 20, 75 mM imidazole). For producing VLPs for conjugation, pellets were thawed and lysed with a cell disruptor in the presence of 2.0 mM PMSF (Sigma). The lysate was spun at 21,000xg for 30 min, filtered with a 0.2 µm filter, and VLPs were isolated by Ni-NTA chromatography using a prepacked HisTrap™ HP column (GE Healthcare). SpyCatcher VLPs were eluted with 2.0 M imidazole, 50 mM glycine, 25 mM sodium citrate, 0.1% Tween 20, pH 8.5. Eluted VLPs were concentrated using an Amicon Ultra 15 mL 30K concentrator (MilliporeSigma) and further purified by SEC using a HiLoad® 16/600 Superdex® 200 (GE Healthcare) column equilibrated with 500 mM glycine pH 8, 250 mM sodium citrate, 1% Tween 20. VLPs were then stored at 4°C and used for up to 1 month for conjugations. SpyCatcher-VLPs precipitated out of solution over time and before use for conjugations, they were either filtered with a 0.2 µm filter or spun down at 21,000g for 10 min.

The pET28a His6-SpyCatcher-mi3 gene (Addgene) was transformed into BL21 (DE3)-RIPL *E.coli* (Agilent). Single colonies were picked and inoculated into an LB overnight starter culture, and grown in 1L LB media until OD 0.8 ($A_{600\ nm}$) with shaking at 220 rpm at 37˚C, after which they were induced with 0.5 mM IPTG and grown for 16-20 hours at 20˚C. Cultures were then harvested and pellets were frozen in lysis buffer (250 mM Tris-HCl pH 8.0, 150 mM NaCl, 50 mM imidazole, 0.02% NaN_3). For producing NPs for conjugation, pellets were thawed and lysed with a cell disruptor in the presence of 2.0 mM PMSF (Sigma), and the lysate was spun at 21,000xg for 30 min, filtered with a 0.2 µm filter, and NPs were isolated by Ni-NTA chromatography using a prepacked HisTrap™ HP column (GE Healthcare), and eluting with 2.0 M imidazole, 20 mM Tris-HCl pH 8, 150 mM NaCl, 0.02% NaN_3. Eluted NPs were concentrated using an Amicon Ultra 15 mL 30K concentrator (MilliporeSigma) and further purified by SEC using a HiLoad® 16/600 Superdex® 200 (GE Healthcare) column equilibrated with 25 mM Tris-HCl pH 8.0, 150 mM NaCl, 0.02% NaN_3. NPs were then stored at 4°C and used for up to 1 month for conjugations. SpyCatcher-NPs precipitated out of solution over time, and before use for conjugations, they were either filtered with a 0.2 µm filter or spun down at 21,000g for 10 min.

Preparation of HA-VLPs and HA-NPs. Purified SpyCatcher-VLPs or SpyCatcher-NPs were incubated with a 1.2-fold molar excess (HA protomer to VLP or NP subunit) of purified SpyTagged HA (either a single HA for making homotypic particles or an equimolar mixture of two or more HAs for making mosaic particles) at room temperature in TBS (25 mM Tris-HCl pH 8.0, 150 mM NaCl, 0.02% NaN_3) overnight. Conjugated VLPs or NPs were then separated from free HA trimers by SEC on a Superose 6 10/300 (GE Healthcare) column equilibrated with PBS (20 mM sodium phosphate pH 7.5, 150 mM NaCl). Fractions corresponding to conjugated VLPS or NPs were collected and analyzed via SDS-PAGE. Concentrations were determined using a Bio-Rad Protein Assay. For stability studies, mosaic-NP preps were stored for a month at 4°C and then analyzed via SEC using a Superose 6 10/300 (GE Healthcare) column equilibrated with PBS (20 mM sodium phosphate pH 7.5, 150 mM NaCl).

EM. HA-conjugated and unconjugated VLPs and NPs were compared by negative-stain EM. Ultrathin, holey carbon-coated, 400 mesh Cu grids (Ted Pella, Inc.) were glow discharged for 60 s at 15 mA. A 3-µl aliquot of SEC-purified HA-VLPs and HA-NPs diluted to approximately 40-100 ug/ml were applied to the grids for 60 s, and then negatively stained with 2% (w/v) uranyl acetate for 30 s. Data were collected with a FEI Tecnai T12 transmission electron microscope at 120 keV at 42,000x magnification.

SEC-purified HA-VLPs and HA-NPs were prepared on grids for cryo-ET using a Mark IV Vitrobot (ThermoFisher Scientific) operated at 21°C and 100% humidity. 3.1 µL of sample was mixed with 1 µL of 10 nm colloidal gold beads (Sigma-Aldrich) as fiducial markers and then applied to 300 mesh Quantifoil R2/2 grids, blotted for 3.5 s, and plunge-frozen in liquid ethane surrounded by liquid nitrogen. Cryo-ET was performed on a 300kV Titan Krios transmission electron microscope (ThermoFisher Scientific) equipped with a Gatan energy filter (slit width 20 eV) operating at a nominal 33,000x magnification. For HA-VLPs, tilt series were collected on a K2 direct electron detector (Gatan) with a pixel size of 2.23 Å•pixel^{-1} using SerialEM software [27], a -3 to -6 µm defocus range, and a total of 98 e^-•Å^{-2} per tilt series. For HA-NPs, tilt series were recorded in counting mode on a K3 direct electron detector (Gatan) with a pixel size of 2.68 Å•pixel^{-1} using SerialEM [27], a -4 to -5 µm defocus range, and a total dose of ~140 e^-•Å^{-2} per tilt series. For both data collections, tilt series images were collected using a dose-symmetric tilt scheme [28] ranging from -60° to 60° with 2° and 3° intervals for HA-VLPs and HA-NPs, respectively. Images were aligned and reconstructed using IMOD [29, 30].

Immunizations. All animal experiments were carried out in 4-6 week old female Balb/c mice obtained from Charles River Laboratories. Immunizations for HA-VLPS and HA-NPs were done in Balb/c mice (n=4 in each group) through intraperitoneal (ip) injections,of 20 ug of antigen in 200 µL of 50% v/v of adjuvant (Sigma Adjuvant System®). For experiments in Figure 4A, mice were immunized on Day 0 and boosted on Day 14. Animals were bled weekly via tail veins. For animals in Figure 5 A, mice were also boosted on Day 37. Mice were then euthanized 2 weeks later (Day 49, 51), bled through cardiac puncture, and spleens were harvested. All blood samples were allowed to clot at room temperature in MiniCollect® Serum and Plasma Tubes (Greiner), and then serum was harvested, frozen in liquid nitrogen, and stored at -80˚C until use. All animal procedures and experiments were performed according to protocols approved by the IACUC.

ELISAs. Nunc® MaxiSorp™ 384-well plates (Sigma) were coated with 10 µg/ml of a purified HA (without a SpyTag) in 0.1 M $NaHC0_3$ pH 9.8 and stored overnight at 4°C. Plates were then blocked with 3% bovine serum albumin (BSA) in TBS-T (TBS with 0.1% Tween 20) for 1 hr at room temperature. Plates were washed with TBS-T after each step. Serum was diluted 1:100 and then serially diluted by 4-fold with TBS-T/3% BSA and added for 3 hr at room temperature. A 1:50,000 dilution of secondary HRP-conjugated goat anti-mouse IgG (Abcam) was added for 1 hr at room temperature. Plates were developed using SuperSignal™ ELISA Femto Maximum Sensitivity Substrate (ThermoFisher) and read at 425 nm. Curves were plotted and integrated to obtain the area under the curve (AUC) using Graphpad Prism 8.3.

In vitro neutralization assays. Neutralization assays were conducted using live PB1flank-eGFP virus for BSL 2 strains A/Aichi/02/1968 (X31; H3N2), A/California/04/2009 (CA09; H1N1), A/Texas/36/1991 (TX91; H1N1), and A/Wisconsin/67/2005 (WI05; H3N2) as described [31] using reagents kindly provided by Dr. Jesse Bloom (Fred Hutchinson). Plasma was set at a top dilution of 1:200 (for Figure 4C) or 1:100 (For Figure 5C) and serially diluted 5-fold (for Figure 4C) or 4-fold (For Figure 5C) for a total of 8 dilutions. Pseudovirus assays were conducted as described [32] for BSL 3 strains A/Shanghai/1/2013 (SH13; H7), A/Jiangxi-Donghu/346/2013 (JX346; H10), A/Vietnam/1203/ 2004 (Viet04; H5N1), and A/Japan/305/1957 (JP57; H2N2). Plasma was set at a top dilution of 1:200 (for Figure 4C) or 1:100 (For Figure 5C) and serially diluted 4-fold for a total of 8 dilutions. Neutralization data were plotted, curves were fit, and ID_{50} values were calculated using Antibody Database [33]. Reported IC_{50}s are geometric means, which are suitable for data sets covering multiple orders of magnitude [34].

Flow cytometry.
Single cell suspension were prepared from immunized mouse spleens by mechanical dissociation using the back of a syringe plunger. Cell suspensions in 70 µm cell strainers were washed in cold RPMI 1640 media and treated with ACK lysing buffer (Gibco) to lyse red blood cells. The resulting white blood cell preparation was resuspended in RPMI 1640 MACS and enriched for memory B cells using the negative selection portion of the protocol in a mouse Memory B Cell Isolation Kit (Miltenyi). Enriched splenocytes were then stained with the following monoclonal antibodies and reagents: CD4-APC-eFluor 780 (clone: RM4-5), F4/80-APC-eFluor 780 (clone: BM8), CD8a-APC-eFluor 780 (clone: 53-6.7), Ly-6G-APC-eFluor 780 (clone: RB6-8C5), IgM-PerCP-eFluor 710 (clone: II/41) (eBioscience), CD19-FITC (clone: 6D5) (Biolegend), IgG1 BV421 (clone: X40), IgG2 BV421 (clone: R19-15) (BD Bioscience), and CA09-HA-APC, Aichi-HA-PEeflour610 and Viet04-HA-PE (prepared as described above). Cell viability was analyzed with Ghost Dye™ Violet 510 (Tonbo). Splenocytes were incubated for 30 min at 4°C in the dark and then washed twice with staining buffer (HBSS, 50 mM HEPES pH 7.4, 2.5 mg/ml BSA, 50 ug/ml DNAse, 1 mM $MgCl_2$). Stained cells were then analyzed with a SY3200 Cell

Sorter (Sony) configured to detect 9 fluorochromes. 500,000-1,000,000 events were collected per sample and analyzed via FlowJo software (TreeStar).

References

1. Krammer F, Smith GJD, Fouchier RAM, Peiris M, Kedzierska K, Doherty PC, Palese P, Shaw ML, Treanor J, Webster RG, Garcia-Sastre A (2018) Influenza. Nat Rev Dis Primers 4(1):3.
2. Sautto GA, Kirchenbaum GA, Ross TM (2018) Towards a universal influenza vaccine: different approaches for one goal. Virology journal 15(1):17.
3. Krammer F (2019) The human antibody response to influenza A virus infection and vaccination. Nat Rev Immunol 19(6):383-97.
4. Air GM (2015) Influenza virus antigenicity and broadly neutralizing epitopes. Current opinion in virology 11:113-21.
5. Angeletti D, Gibbs JS, Angel M, Kosik I, Hickman HD, Frank GM, Das SR, Wheatley AK, Prabhakaran M, Leggat DJ, McDermott AB, Yewdell JW (2017) Defining B cell immunodominance to viruses. Nat Immunol 18(4):456-63.
6. Schmidt AG, Therkelsen MD, Stewart S, Kepler TB, Liao HX, Moody MA, Haynes BF, Harrison SC (2015) Viral receptor-binding site antibodies with diverse germline origins. Cell 161(5):1026-34.
7. Ekiert DC, Bhabha G, Elsliger MA, Friesen RH, Jongeneelen M, Throsby M, Goudsmit J, Wilson IA (2009) Antibody recognition of a highly conserved influenza virus epitope. Science 324(5924):246-51.
8. Joyce MG, Wheatley AK, Thomas PV, Chuang GY, Soto C, Bailer RT, Druz A, Georgiev IS, Gillespie RA, Kanekiyo M, Kong WP, Leung K, Narpala SN, Prabhakaran MS, Yang ES, Zhang B, Zhang Y, Asokan M, Boyington JC, Bylund T, Darko S, Lees CR, Ransier A, Shen CH, Wang L, Whittle JR, Wu X, Yassine HM, Santos C, Matsuoka Y, Tsybovsky Y, Baxa U, Program NCS, Mullikin JC, Subbarao K, Douek DC, Graham BS, Koup RA, Ledgerwood JE, Roederer M, Shapiro L, Kwong PD, Mascola JR, McDermott AB (2016) Vaccine-Induced Antibodies that Neutralize Group 1 and Group 2 Influenza A Viruses. Cell 166(3):609-23.
9. Lang S, Xie J, Zhu X, Wu NC, Lerner RA, Wilson IA (2017) Antibody 27F3 Broadly Targets Influenza A Group 1 and 2 Hemagglutinins through a Further Variation in VH1-69 Antibody Orientation on the HA Stem. Cell reports 20(12):2935-43.
10. Tan HX, Jegaskanda S, Juno JA, Esterbauer R, Wong J, Kelly HG, Liu Y, Tilmanis D, Hurt AC, Yewdell JW, Kent SJ, Wheatley AK (2019) Subdominance and poor intrinsic immunogenicity limit humoral immunity targeting influenza HA stem. J Clin Invest 129(2):850-62.
11. Impagliazzo A, Milder F, Kuipers H, Wagner MV, Zhu X, Hoffman RM, van Meersbergen R, Huizingh J, Wanningen P, Verspuij J, de Man M, Ding Z, Apetri A, Kukrer B, Sneekes-Vriese E, Tomkiewicz D, Laursen NS, Lee PS, Zakrzewska A, Dekking L, Tolboom J, Tettero L, van Meerten S, Yu W, Koudstaal W, Goudsmit J, Ward AB, Meijberg W, Wilson IA, Radosevic K (2015) A stable trimeric influenza hemagglutinin stem as a broadly protective immunogen. Science 349(6254):1301-6.
12. Yassine HM, Boyington JC, McTamney PM, Wei CJ, Kanekiyo M, Kong WP, Gallagher JR, Wang L, Zhang Y, Joyce MG, Lingwood D, Moin SM, Andersen H, Okuno Y, Rao SS, Harris AK, Kwong PD, Mascola JR, Nabel GJ, Graham BS (2015) Hemagglutinin-stem nanoparticles generate heterosubtypic influenza protection. Nat Med 21(9):1065-70.
13. Nachbagauer R, Liu WC, Choi A, Wohlbold TJ, Atlas T, Rajendran M, Solorzano A, Berlanda-Scorza F, Garcia-Sastre A, Palese P, Albrecht RA, Krammer F (2017) A universal influenza virus vaccine candidate confers protection against pandemic H1N1 infection in preclinical ferret studies. NPJ Vaccines 2:26.

14. Liu WC, Nachbagauer R, Stadlbauer D, Solorzano A, Berlanda-Scorza F, Garcia-Sastre A, Palese P, Krammer F, Albrecht RA (2019) Sequential Immunization With Live-Attenuated Chimeric Hemagglutinin-Based Vaccines Confers Heterosubtypic Immunity Against Influenza A Viruses in a Preclinical Ferret Model. Front Immunol 10:756.
15. Weidenbacher PA, Kim PS (2019) Protect, modify, deprotect (PMD): A strategy for creating vaccines to elicit antibodies targeting a specific epitope. Proc Natl Acad Sci U S A 116(20):9947-52.
16. Kanekiyo M, Joyce MG, Gillespie RA, Gallagher JR, Andrews SF, Yassine HM, Wheatley AK, Fisher BE, Ambrozak DR, Creanga A, Leung K, Yang ES, Boyoglu-Barnum S, Georgiev IS, Tsybovsky Y, Prabhakaran MS, Andersen H, Kong WP, Baxa U, Zephir KL, Ledgerwood JE, Koup RA, Kwong PD, Harris AK, McDermott AB, Mascola JR, Graham BS (2019) Mosaic nanoparticle display of diverse influenza virus hemagglutinins elicits broad B cell responses. Nat Immunol 20(3):362-72.
17. Brune KD, Howarth M (2018) New Routes and Opportunities for Modular Construction of Particulate Vaccines: Stick, Click, and Glue. Front Immunol 9:1432.
18. Brune KD, Leneghan DB, Brian IJ, Ishizuka AS, Bachmann MF, Draper SJ, Biswas S, Howarth M (2016) Plug-and-Display: decoration of Virus-Like Particles via isopeptide bonds for modular immunization. Scientific reports 6:19234.
19. Bruun TUJ, Andersson AC, Draper SJ, Howarth M (2018) Engineering a Rugged Nanoscaffold To Enhance Plug-and-Display Vaccination. ACS Nano 12(9):8855-66.
20. Zakeri B, Fierer JO, Celik E, Chittock EC, Schwarz-Linek U, Moy VT, Howarth M (2012) Peptide tag forming a rapid covalent bond to a protein, through engineering a bacterial adhesin. Proc Natl Acad Sci U S A 109(12):E690-7.
21. Escolano A, Gristick HB, Abernathy ME, Merkenschlager J, Gautam R, Oliveira TY, Pai J, West AP, Jr., Barnes CO, Cohen AA, Wang H, Golijanin J, Yost D, Keeffe JR, Wang Z, Zhao P, Yao KH, Bauer J, Nogueira L, Gao H, Voll AV, Montefiori DC, Seaman MS, Gazumyan A, Silva M, McGuire AT, Stamatatos L, Irvine DJ, Wells L, Martin MA, Bjorkman PJ, Nussenzweig MC (2019) Immunization expands B cells specific to HIV-1 V3 glycan in mice and macaques. Nature 570(7762):468-73.
22. Whittle JR, Wheatley AK, Wu L, Lingwood D, Kanekiyo M, Ma SS, Narpala SR, Yassine HM, Frank GM, Yewdell JW, Ledgerwood JE, Wei CJ, McDermott AB, Graham BS, Koup RA, Nabel GJ (2014) Flow cytometry reveals that H5N1 vaccination elicits cross-reactive stem-directed antibodies from multiple Ig heavy-chain lineages. J Virol 88(8):4047-57.
23. Mostafa A, Abdelwhab EM, Mettenleiter TC, Pleschka S (2018) Zoonotic Potential of Influenza A Viruses: A Comprehensive Overview. Viruses 10(9).
24. Shishovs M, Rumnieks J, Diebolder C, Jaudzems K, Andreas LB, Stanek J, Kazaks A, Kotelovica S, Akopjana I, Pintacuda G, Koning RI, Tars K (2016) Structure of AP205 Coat Protein Reveals Circular Permutation in ssRNA Bacteriophages. J Mol Biol 428(21):4267-79.
25. Hsia Y, Bale JB, Gonen S, Shi D, Sheffler W, Fong KK, Nattermann U, Xu C, Huang PS, Ravichandran R, Yi S, Davis TN, Gonen T, King NP, Baker D (2016) Design of a hyperstable 60-subunit protein dodecahedron. [corrected]. Nature 535(7610):136-9.
26. Ekiert DC, Friesen RH, Bhabha G, Kwaks T, Jongeneelen M, Yu W, Ophorst C, Cox F, Korse HJ, Brandenburg B, Vogels R, Brakenhoff JP, Kompier R, Koldijk MH, Cornelissen LA, Poon LL, Peiris M, Koudstaal W, Wilson IA, Goudsmit J (2011) A highly conserved neutralizing epitope on group 2 influenza A viruses. Science 333(6044):843-50.
27. Mastronarde DN (2005) Automated electron microscope tomography using robust prediction of specimen movements. J Struct Biol 152(1):36-51.
28. Hagen WJH, Wan W, Briggs JAG (2017) Implementation of a cryo-electron tomography tilt-scheme optimized for high resolution subtomogram averaging. J Struct Biol 197(2):191-8.
29. Kremer JR, Mastronarde DN, McIntosh JR (1996) Computer visualization of three-dimensional image data using IMOD. J Struct Biol 116(1):71-6.

30. Mastronarde DN, Held SR (2016) Automated tilt series alignment and tomographic reconstruction in IMOD. J Struct Biol.
31. Bloom JD, Gong LI, Baltimore D (2010) Permissive secondary mutations enable the evolution of influenza oseltamivir resistance. Science 328(5983):1272-5.
32. Temperton NJ, Hoschler K, Major D, Nicolson C, Manvell R, Hien VM, Ha do Q, de Jong M, Zambon M, Takeuchi Y, Weiss RA (2007) A sensitive retroviral pseudotype assay for influenza H5N1-neutralizing antibodies. Influenza Other Respir Viruses 1(3):105-12.
33. West AP, Jr., Scharf L, Horwitz J, Klein F, Nussenzweig MC, Bjorkman PJ (2013) Computational analysis of anti-HIV-1 antibody neutralization panel data to identify potential functional epitope residues. Proc Natl Acad Sci U S A 110(26):10598-603.
34. Sheskin D (2004) Handbook of Parametric and Nonparametric Statistical Procedures. 3rd ed. Boca Raton: Chapman & Hall/CRC. 1193 p.

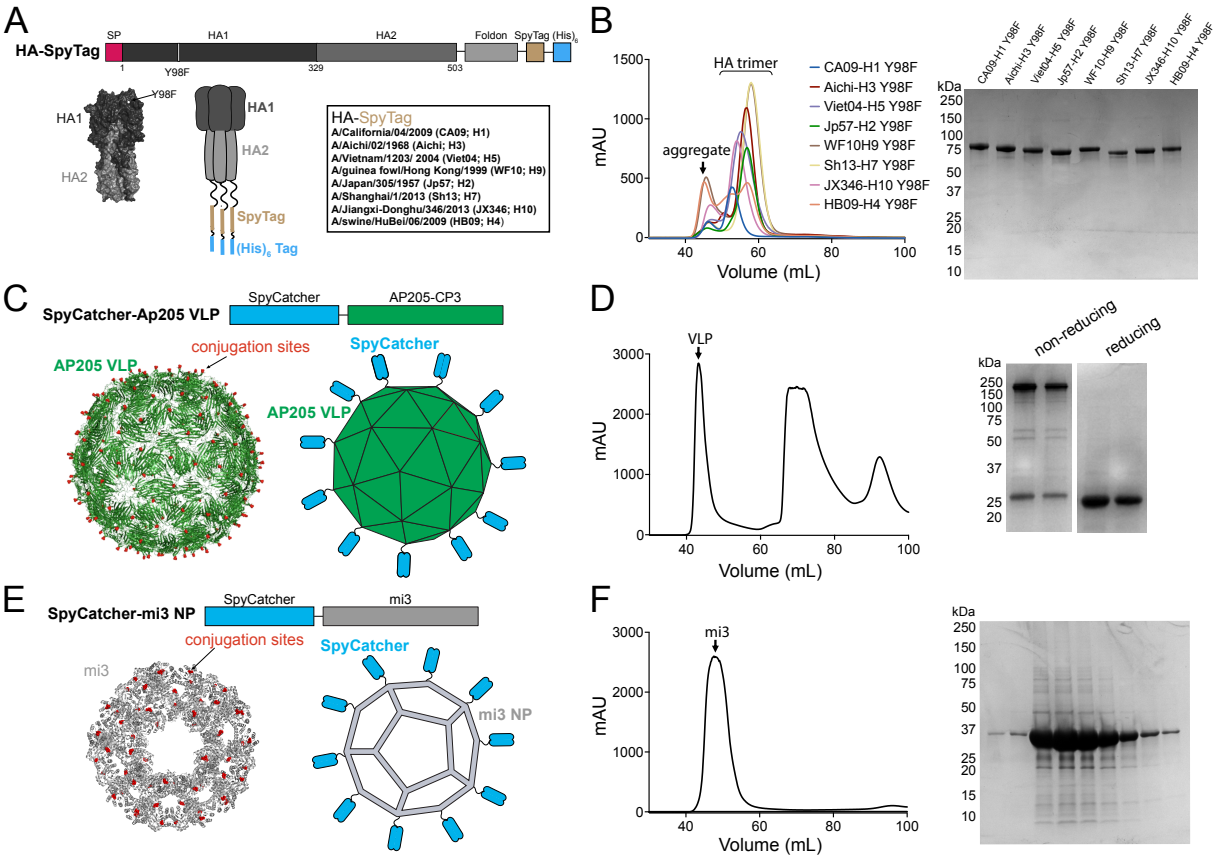

Figure 1. Design and characterization of SpyTagged HAs, SpyCatcher VLPs, and SpyCatcher-NPs. A. Top: Schematic of the SpyTagged HA construct (SP = signal peptide). The HA2 ectodomain is followed by a foldon trimerization domain from T4 fibritin, a 13-residue SpyTag, and a 6x-His tag. Amino acids are numbered according to the H3 nomenclature. Horizontal lines represent Gly_4Ser linkers. Bottom: Surface representation of an HA trimer structure (PDB 3VUN), schematic of a SpyTagged HA, and list of influenza strains from which SpyTagged HAs were derived. **B**. SEC profiles and reducing SDS-PAGE analysis of 8 different purified SpyTagged HAs including the Y98F substitution. **C**. SpyCatcher-AP205 VLPs. Top: Schematic of construct. Bottom: EM structure of T=3 AP205 particle (PDB 5FS3) [24] with the locations of SpyCatcher fusion sites indicated by red dots (left) and schematic SpyCatcher-VLP (right). **D**. Purification of SpyCatcher-VLPs. Left: SEC profile with peak representing properly-assembled VLPs indicated. Right: Reducing and non-reducing SDS-PAGE of fractions corresponding to VLP peak. **E**. SpyCatcher-mi3 NPs. Top: schematic of construct. Bottom: EM structure of I3-01 particle related to mi3 [25] with the locations of SpyCatcher fusion sites indicated by red dots (left) and schematic SpyCatcher-NP (right). **F**. Purification of SpyCatcher-NPs. Left: SEC profile. Right: Reducing SDS-PAGE of fractions corresponding to mi3 NP peak.

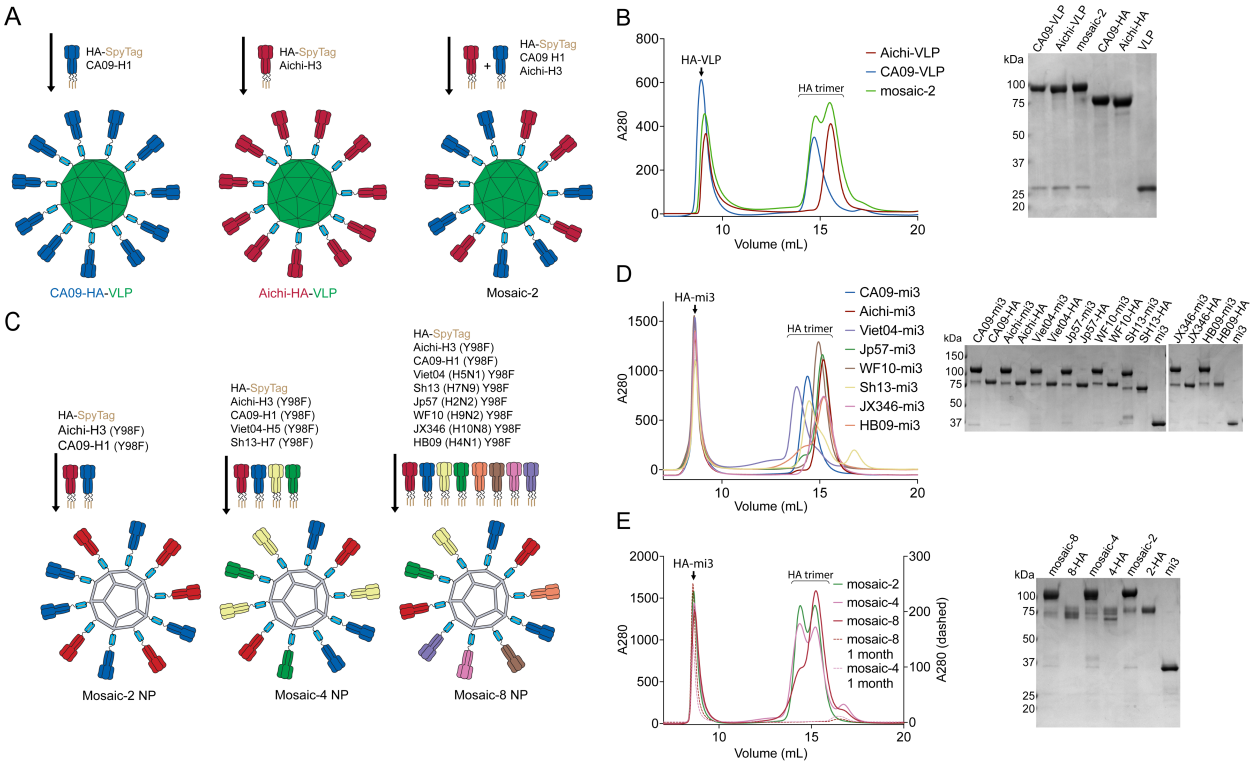

Figure 2. Conjugation of SpyCatcher-VLPs and -NPs. A. SpyCatcher-AP205-VLP conjugations with SpyTagged-HA trimers. **B**. Purification of conjugated SpyCatcher-VLPs. Left: SEC separation of conjugated VLPs from free HA trimers. Right: Reducing SDS-PAGE analysis of VLPs and purified HAs. **C**. SpyCatcher-mi3-NP conjugations with SpyTagged-HA_Y98F mutant trimers. **D**. Purification of homotypic SpyCatcher-NPs. Left: SEC separation of conjugated NPs from free HA trimers. Right: Reducing SDS-PAGE analysis of NPs and purified HAs. **E**. Purification of heterotypic mosaic-NPs. Left: SEC separation of conjugated NPs from free HA trimers, including SEC profile of purified conjugated NPs after 1 month storage at 4 ˚C. Right: Reducing SDS-PAGE analysis of NPs and purified HAs.

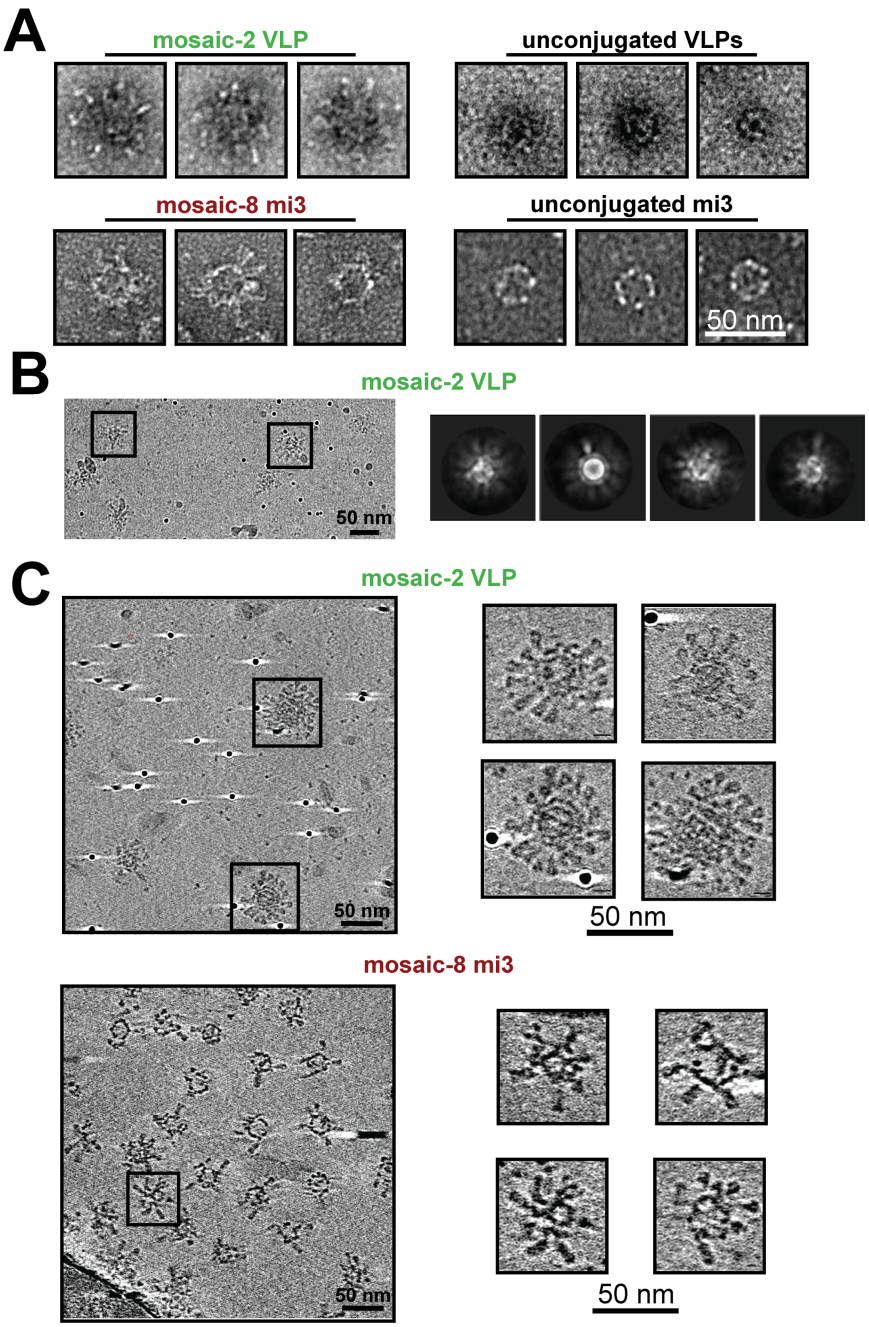

Figure 3. EM of conjugated VLPs and NPs. Scale bars shown apply to all images in each panel. **A.** Negative-stain EM of HA-conjugated VLPs and mi3 NPs compared with unconjugated counterparts. **B.** Cryo-EM micrograph of HA-VLP sample (left) and representative 2D class averages (right). Densities for HA trimers are blurry in the class averages, likely because the trimers occupy different positions on individual particles. **C.** Cryo-ET imaging of HA particles. Computationally-derived tomographic slices of HA-VLP (top panels; 2.78 nm slices) and HA-NP (bottom panels; 3.21 nm slices). Slices derived from the widest portions of representative particles are shown to the right in each panel.

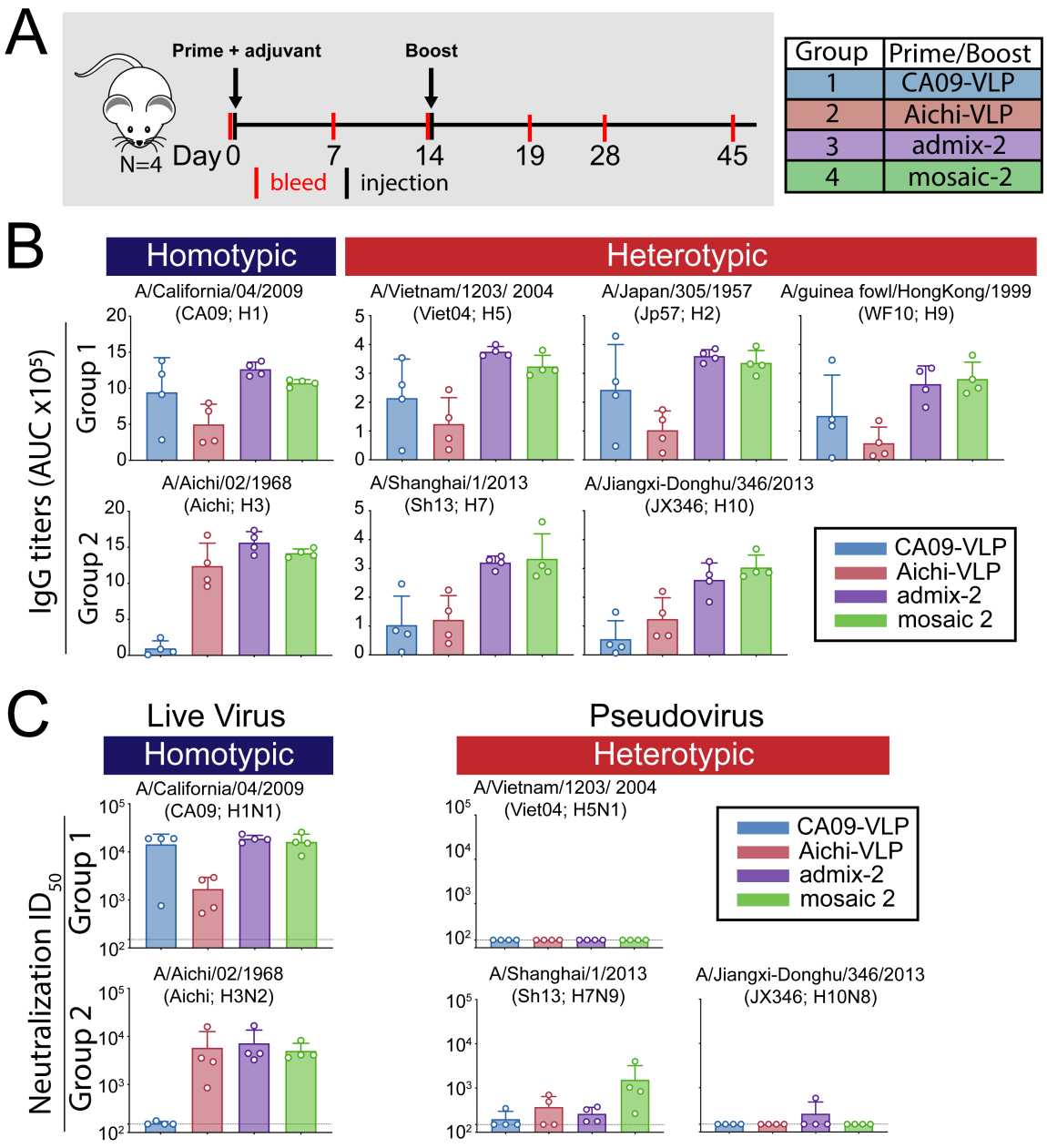

Figure 4. Immunizations with HA-VLPs. **A**. Schematic of the immunization protocol (four animals per injection). **B**. Serum antibody response to HA shown by ELISA binding as area under the curve (AUC) of Day 28 serum to Group 1 and Group 2 HA trimers. Each dot represents serum from one animal, with arithmetic means and standard deviations represented by rectangles and horizontal lines, respectively. Homotypic strains (present on the mosaic-2 VLP) and heterotypic strains (not present on the mosaic-2 VLP) are indicated by the blue and red rectangles, respectively, above the ELISA data. Bottom right: Color coding for data. **C**. Serum neutralization titers from Day 45 determined by in vitro neutralization assays using live virus or pseudoviruses. Each dot represents serum from one animal, with geometric mean and geometric standard deviations represented by rectangles and horizontal lines, respectively. Dotted lines indicate limits of detection.

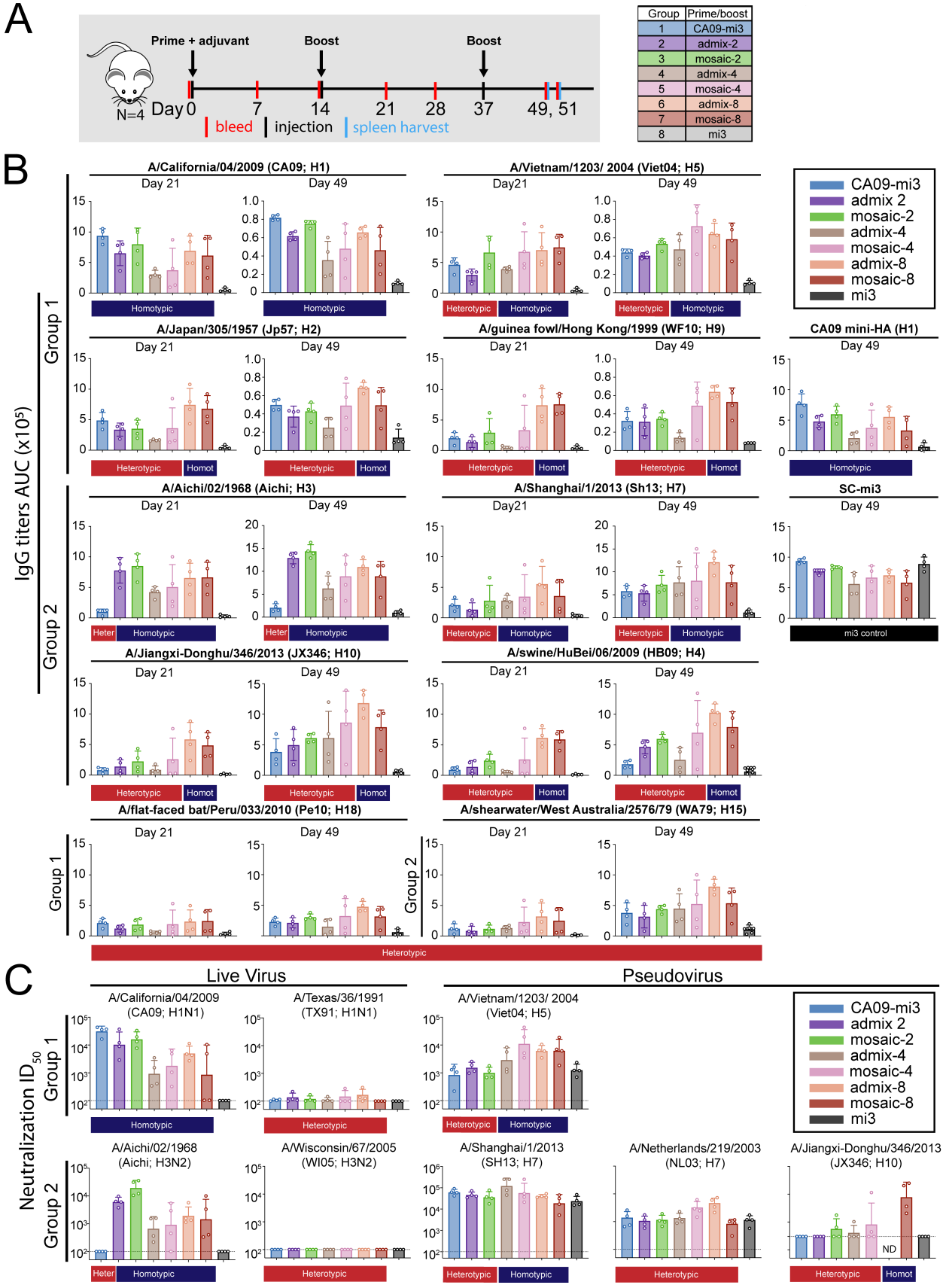

Figure 5. Immunizations with HA-NPs. **A**. Schematic of the immunization protocol (four animals per injection). **B**. Serum antibody response to HA shown by ELISA binding as area under the curve (AUC) of Day 21 and Day 49 serum to recombinant Group 1 and Group 2 HA trimers. Each dot represents serum from one animal, with means and standard deviations represented by rectangles and horizontal lines, respectively. Homotypic strains that were present on the mosaic NPs and heterotypic strains that were not present are indicated by the blue and red rectangles, respectively, above the ELISA data. Top right: Color coding for data. **C**. Serum neutralization titers from Day 45 determined by in vitro neutralization assays using live virus or pseudoviruses. Each dot represents serum from one animal, with geometric means and geometric standard deviations represented by rectangles and horizontal lines, respectively. Dotted lines indicate limits of detection. Top right: Color coding for data.

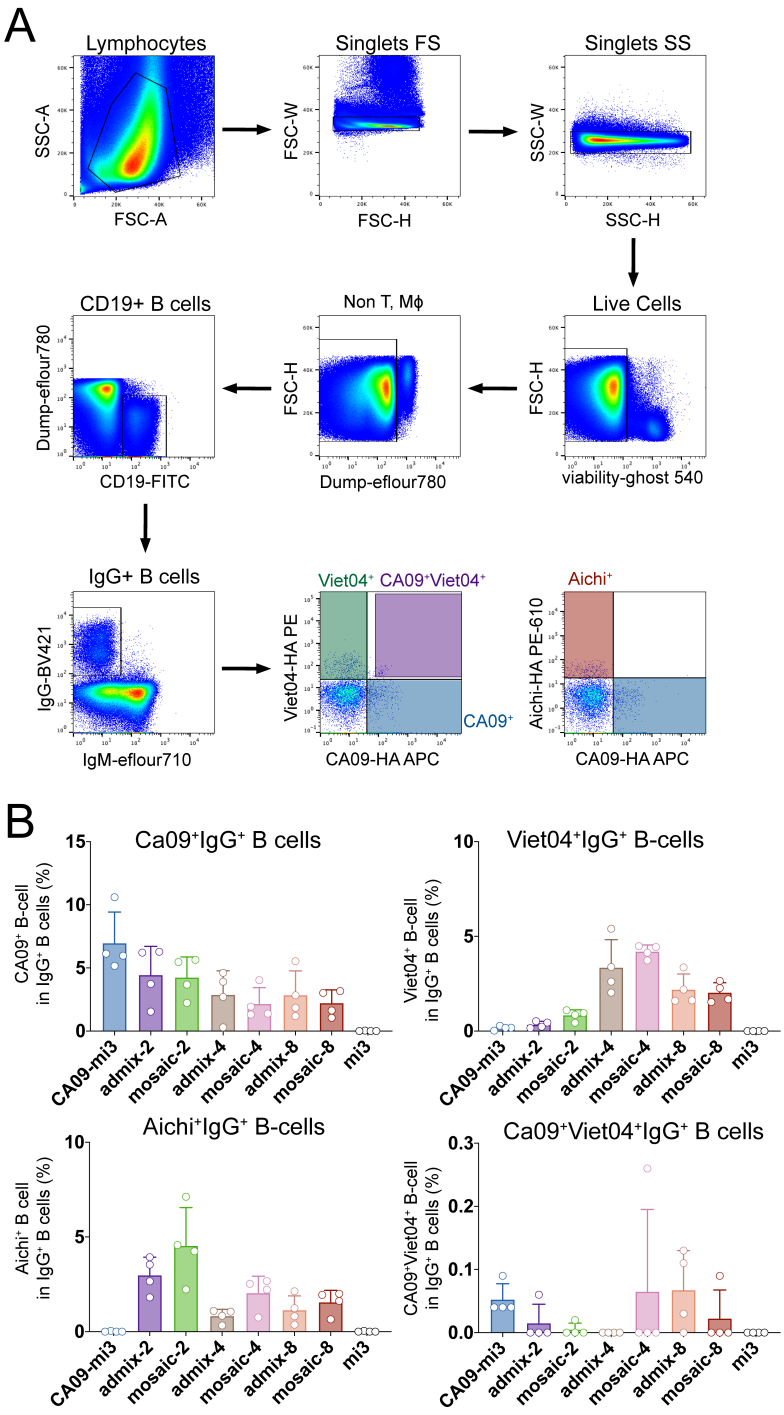

Figure 6. B cell responses induced by mosaic NP immunizations. A. Gating strategy for flow cytometry experiments using single cell suspension from spleens harvested from immunized mice in Figure 5A. Anti-CD3, anti-CD8, anti-F4/80, and anti-Ly6G were used to remove T cells, macrophages, monocytes, and neutrophils. Cells were then gated to isolate CD19/IgG-positive and IgM-negative, which were probed for binding of CA09-HA-APC (allophycocyanin), Aichi-HA-PE-eFluor610 (phycoerythrin-eFluor 610), and/or Viet04-HA-PE (phycoerythrin). **B**. Percent CA09+, Viet04+, Aichi+, and CA09+/Viet04+ in IgG+ B cells plotted for each group.